

# Investigation of Specimen Geometry Effects and Material Inhomogeneity Effects in A533B Steel

**James A. Joyce<sup>1</sup> and R.L. Tregoning<sup>2</sup>**

<sup>1</sup> US Naval Academy, Annapolis, MD USA

<sup>2</sup> Naval Surface Warfare Center, Carderock, MD USA

**ABSTRACT:** *The Master Curve method and the associated reference temperature, as defined in the new test standard ASTM E1921, is rapidly moving from the research laboratory to applications in the U.S. commercial nuclear power industry. The  $T_o$  reference temperature is very robust, and it has rapidly become a tool to investigate material inhomogeneity effects and constraint effects because it is capable of measuring differences imperceptible using earlier methods that have been used to define the ductile-to-brittle transition in structural ferritic steels. Previous work by the present authors[1-2] has shown that  $T_o$  is sensitive to the specimen geometry used in its evaluation. While this geometry sensitivity is expected if shallow crack specimens are compared with deep crack specimens, a significant difference also appears to exist between deep crack C(T) and SE(B) geometries. This difference causes concern in the application of ASTM E1921 to regulatory decisions facing the US Nuclear Regulatory Commission. In this work a study is made to separate the effects of material inhomogeneity and specimen geometry for the same A533B pressure vessel material studied extensively in the previous work. The results show that the  $T_o$  differences due to material inhomogeneity can be separated from that due to specimen geometry, at least if the data set utilized is extensive enough.*

## INTRODUCTION

The recently developed Master Curve and the associated  $T_o$  reference temperature have provided a much improved method to quantitatively define the ductile-to-brittle transition temperature in ferritic structural steels. This is especially important in the commercial nuclear power industry in the United States. United States Code of Federal Regulations Part 10 § 50.61 documents the current procedures used to assess the fracture integrity of the nuclear reactor pressure vessel during a pressurized thermal shock event using  $RT_{NDT}$ . The replacement of the  $RT_{NDT}$ , based on a correlation of CVN and NDT data, with the much more robust fracture mechanics based Master Curve reference temperature,  $T_o$ , will greatly aid in making these decisions. Nonetheless certain difficulties remain, one of which is the apparent dependence of the Master Curve reference temperature on the

specimen geometry used for its evaluation. This dependence was reported by the present authors[1-2] for an A533B nuclear pressure vessel steel, and also by Wallin[3] using the EURO Fracture Toughness data set (A508 Cl.2)[4]. An application of constraint correction methodologies[5] as proposed by Gao and Dodds[6] appears to show that the magnitude of the differences demonstrated between standard C(T) and SE(B) specimen geometries in this A533B steel cannot be explained using the present constraint adjustment procedures. In this work 108 pre-cracked Charpy specimens are used to characterize the dependence of the  $T_0$  reference temperature on crack position through a thick, inhomogeneous A533B pressure vessel plate, and this set of results is compared to 201 fracture toughness tests obtained previously using SE(B) and C(T) geometry specimens. The results show that if a very large data set is available the difference in  $T_0$  between C(T) and SE(B) geometries can easily be separated from the effect of material inhomogeneity.

## **EXPERIMENTAL DETAILS**

The A533B test material, designated by the material code HEW, was extracted from a portion of shell plate from the decommissioned Shoreham nuclear plant boiling water reactor pressure vessel. The test piece was originally located in the upper section of the vessel just below the nozzle inserts. The vessel wall plate thickness is 150 mm (6 inch) with a 6 mm (0.25 inch) thick stainless steel cladding on the inner surface. All fracture mechanics specimens tested in this study were oriented in the L-S orientation as defined in ASTM E399, while all tensile specimens were oriented in the L direction.

### ***Tensile Properties***

The chemistry and tensile-mechanical properties of this steel at four temperatures are presented in reference [2]. Forty 6.2 mm diameter tensile specimens were machined from this material and tested at three temperatures,  $-80^{\circ}\text{C}$ ,  $24^{\circ}\text{C}$  (ambient), and  $120^{\circ}\text{C}$ . The resulting yield, ultimate strengths, % elongation and % reduction of area are shown plotted in Figure 1 as a function of position through the plate. The dashed lines in these figures represent the through-thickness average properties for each measurement. It is clear from these plots that these material properties vary with temperature, but do not appear to be a function of the plate thickness location with the possible exception of the material in a 5 to 10 mm. surface zone not sampled by this test matrix.

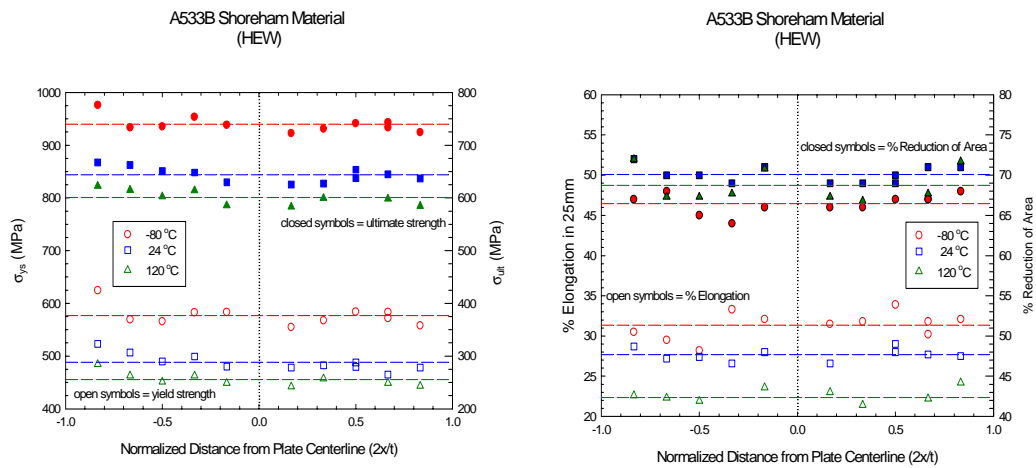


**Figure 1** Tensile and ductility properties plotted versus distance from the plate centerline for HEW A533B steel.

### *Fracture Toughness*

A few standard C(T) specimens were used to provide an indication of the upper shelf material toughness of the A533B steel. Standard J-R curve testing was conducted under quasi-static loading at room temperature. The results indicate that the A533B material has a high upper shelf toughness with an average material toughness ( $J_Q = 250 \text{ kJ/m}^2$ ) that substantially exceeds the E1820 size criteria for a 1T specimen, and is therefore not a valid, size independent  $J_{Ic}$  measure.

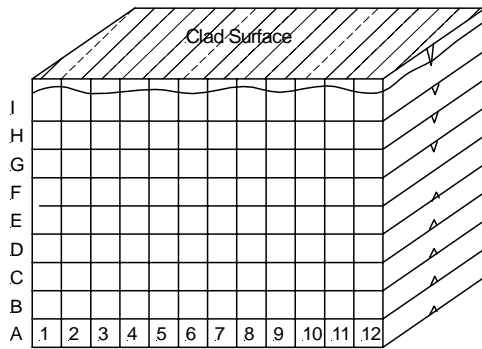
### *Master Curve*

A large test matrix has been conducted for the HEW A533B steel over the past three years. The test matrix containing the specimen geometries evaluated and the chosen test temperatures is summarized in Table 1. This table summarizes the current database of 201 standard fracture toughness values for this material of which 175 results are uncensored as per ASTM E1921 requirements. The test matrix is comprehensive in that all the typical test geometries were evaluated at more than one test temperature with respect to the best estimate  $T_0$ . Three distinct specimen geometries were studied: a square cross-section single-edged notch bend geometry, a standard rectangular cross-section single-edged notch bend {SE(B)} geometry, and the compact tension {C(T)} geometry.

The planar dimensions for each specimen type scale self-similarly with respect to  $B_{max}$  so that the specimen width (W) to  $B_{max}$  ratio is constant for each geometry regardless of absolute specimen size. The  $W/B = 2$  for the C(T) and SE(B) specimens, while  $W/B = 1$  for the square cross section

bend geometries. All specimens were oriented with the crack in the L-S direction as defined by ASTM E399. Further information on this test plan is available in reference [2].

To investigate the dependence of  $T_o$  on through plate specimen position in this thick plate, a total of 108 Charpy size SE(B) specimens were machined from the plate material as shown in Figure 2, precracked to  $a/W = 0.5$ , and subsequently side grooved using a Charpy notch configuration to a total thickness reduction of 20%. The “I” layer contained the clad material. These specimens were precracked until the crack tip extended approximately 0.25 mm into the base material beyond the clad. Test temperatures were chosen to meet the requirements of E1921. All layers



except the B layer generated a valid single temperature estimate of  $T_o$ . When all specimens from a single layer were analyzed using a multitemperature analysis, each yielded an ASTM-valid  $T_o$  estimate. The multi-temperature estimates were used in all comparisons made in the discussion section below.

**Figure 2** Cutting diagram for A533B(HEW) precracked Charpy specimens.

## PRESENTATION OF RESULTS

A summary of the C(T) and SE(B) data sets and results is presented in Table 1. Figure 3 gives an overall view of these extensive data sets. Multi-temperature evaluations of the  $T_o$  reference temperatures using the procedure of ASTM E1921 gives  $T_o = -75.4^{\circ}\text{C}$  for the C(T) geometry data sets and  $T_o = -91.6^{\circ}\text{C}$  for the SE(B) data sets, excluding the precracked Charpy results. Clearly, data from both geometries agree well with the E1921 master curve shape confidence bounds, but the two geometries give  $T_o$  reference temperatures different by  $16.2^{\circ}\text{C}$ .

The results of the precracked Charpy tests are tabulated in Table 2 and plotted in Figure 4 versus the standard master curve and 95% confidence bounds. Application of E1921 to the 108 precracked Charpy specimen results gives a multi-temperature  $T_o = -112.8^{\circ}\text{C}$  and, by choosing minimal sets of six specimens out of the set of 108 data sets available according to E1921, extreme values of  $T_o$  from  $-145.5^{\circ}\text{C}$  to  $-67.4^{\circ}\text{C}$  can be

**Table 1 C(T) and SE(B) Data Summary**

Specimen Geometry	Size	Test Temperature °C	N	r	T <sub>0</sub> °C	E1921 Validity
C(T)	0.5T	-39	13	6	-84.0	Yes
C(T)	0.5T	-86	8	8	-79.5	Yes
C(T)	0.5T	-40	8	7	-57.8	Yes
C(T)	0.5T	-118	6	6	-83.7	Yes
C(T)	1T	-40	14	14	-74.9	Yes
C(T)	1T	-85	8	8	-82.0	Yes
C(T)	1T	-110	8	8	-69.9	Yes
C(T)	1T	-60	6	6	-73.8	Yes
C(T)	1T	-25	8	8	-67.8	Yes
C(T)	0.1T	-11	4	1	-93.2	No
C(T)	0.8T	-80	7	7	-76.0	Yes
C(T)	0.8T	-60	7	7	-84.4	Yes
SE(B)	0.5T	-40	6	2	-92.8	No
SE(B)	0.5T	-50	6	3	-94.0	No
SE(B)	0.5T	-60	6	6	-82.3	Yes
SE(B)	0.5T	-79	8	7	-101.7	Yes
SE(B)	0.5T	-116	8	8	-87.1	Yes
SE(B)	0.5T	-81	8	6	-94.1	Yes
SE(B)	0.5T	-115	7	7	-98.5	Yes
SE(B)	1T	-12	7	4	-80.2	No
SE(B)	1T	-27	6	6	-83.5	Yes
SE(B)	1T	-42	12	12	-86.5	Yes
SE(B)	1T	-118	10	10	-95.4	Yes
SE(B)	1T Square	-118	8	8	-93.7	Yes
SE(B)	1T Square	-76	8	8	-93.6	Yes
SE(B)	1T Square	-50	12	9	-90.5	Yes

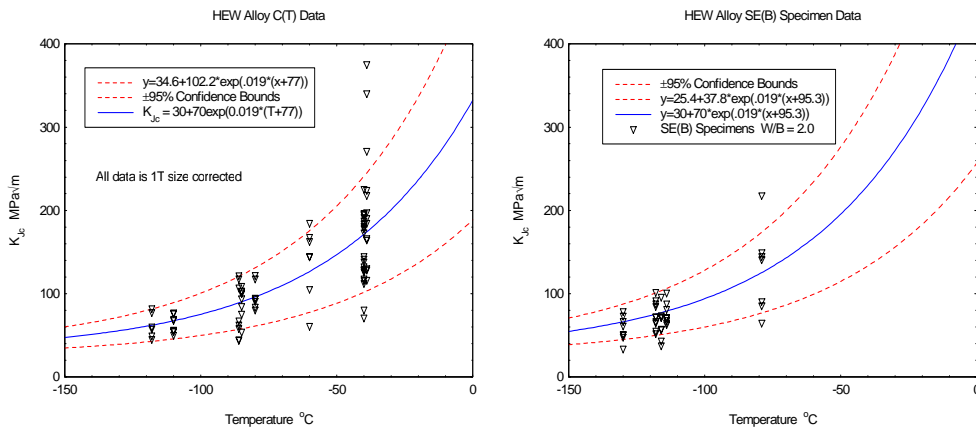


**Figure 3** Toughness in the a) C(T) and b) SE(B) geometries.

**Table 2 HEW Precracked Charpy Result Summary**

Specimen Layer	Test Temperature °C	N	r	T <sub>0</sub> Single Temp. °C	E1921 Validity	T <sub>0</sub> Multi-Temp. °C	E1921 Validity
A	-140	9	9	-141.	Yes	-141.6	Yes
B	-110	8	5	-115.	No	-113.6	Yes
B	-90	3	1	---	No		
C	-110	12	11	-102.	Yes	-100.4	Yes
D	-100	8	8	-83.0	Yes	-81.7	Yes
D	-90	4	4	-81.0	No		
E	-100	12	12	-91.7	Yes	-90.5	Yes
F	-110	8	8	-85.4	Yes	-81.7	Yes
F	-95	4	4	-80.5	No		
G	-110	8	8	-84.8	Yes	-87.0	Yes
G	-95	4	3	-94.2	No		
H	-110	8	8	-87.9	Yes	-85.7	Yes
H	-96	3	3	-86.2	No		
I	-125	10	9	-117.4	Yes	-120.2	Yes

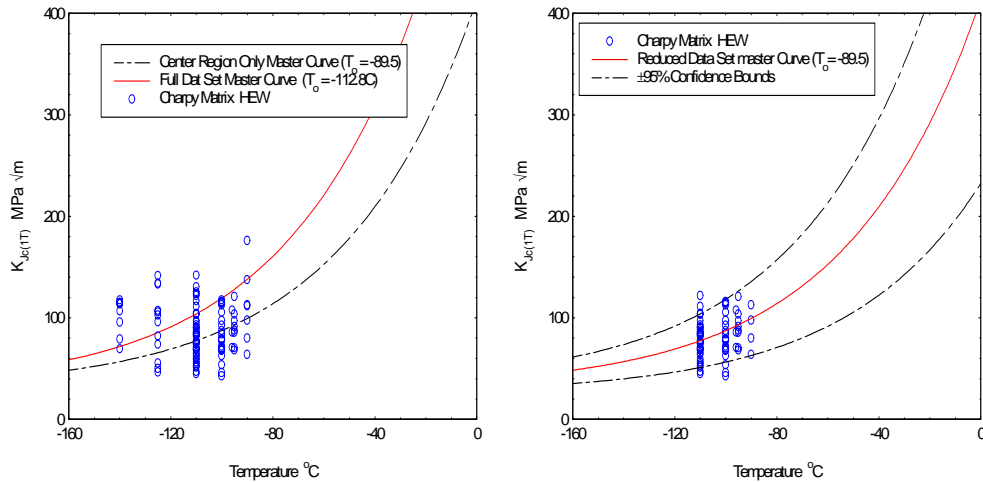


**Figure 4** Summary of Charpy data including (a) all eight layers and (b) the center five of the eight layers.

estimated. The resulting 78°C range dramatically exceeds the expected 20 to 30°C range of E1921 and the best estimate of  $T_0 = -112.8^\circ\text{C}$  is very non-conservative when compared to results obtained from C(T) and SE(B)

specimen data sets. Nonetheless, this HEW material is more uniform than another A533B vessel material reported previously[7].

Figure 4a also shows that the combined precracked Charpy data does not correspond well with either the master curve shape or the E1921 confidence interval. However, eliminating the data obtained from specimens obtained near the plate surface layers (layers A, B, and I) results in good correspondence between the data and the E1921 master curve median and confidence bound predictions (Figure 4b). Also, the multi-temperature  $T_o = -89.5^{\circ}\text{C}$ , is similar to the SE(B) result ( $-91.6^{\circ}\text{C}$ ) presented above.

In order to separate the effects of geometry and material homogeneity, the crack position through the plate thickness was determined from specimen machining drawings for all of the C(T) and SE(B) specimens utilized in Table 3. All of these specimens were identified as being in “bins” corresponding to the crack tip position, using the A through I notation of Figure 2. While the crack tips in the Charpy specimens were restricted to the center area of these “bins”, the C(T) and SE(B) specimens were located in a bin if their post fatigue crack tip was located anywhere in the particular A through I region. The E1921 multi-temperature procedure was then applied to each bin, keeping C(T) and SE(B) geometries separate. These results are summarized in Table 3 and Figure 5. It is clear that the C(T) versus SE(B) difference persists as the reference temperature changes through the thickness of the A533B vessel wall. The difference between the C(T) and SE(B) geometries of each layer varies from  $10.1^{\circ}\text{C}$  to  $18.6^{\circ}\text{C}$ , while the precracked Charpy result is generally intermediate to C(T) and SE(B) results, tending to fall more closely to the SE(B) data.

## CONCLUSIONS

- For this material at least,  $T_o$  is dramatically different for measurements made with C(T) and SE(B) specimen geometries.
- The difference in measured  $T_o$  between C(T) and SE(B) specimen geometries persists through the material plate thickness even as the measured  $T_o$  changes dramatically.
- Precracked Charpy, surveillance size specimens give  $T_o$  generally intermediate to the C(T) and SE(B) results, corresponding more closely to the standard SE(B) measurements.
- The strong variation of  $T_o$  with position through the thickness of this plate is not suggested by the standard tensile mechanical properties.

## REFERENCES

1. Joyce, J.A., Tregoning, R.L., (2000), ECF13, San Sebastian.
2. Tregoning, R.L., Joyce, J.A., (2000), PVP Vol. 412, ASME, Seattle.
3. Wallin, K., (2001), PVP Vol. 423, 157, ASME, Atlanta.
4. Heerens, J., Hellmann, D., (1999), *MAT1-CT-940080 Final Report*, GKSS, Geesthacht.
5. Joyce, J.A., Tregoning, R.L., (2001), *Proc. 31<sup>st</sup> Nat. Symp. Fat. And Frac., ASTM, Grand Tetons.*
6. Gao, X., Dodds, R.H., (2000), *Eng. Fracture Mechanics*, **67**, 101.
7. Zhang, X.J., Tregoning, R.L., (1999) *Proc. Int. Symp. On Steel for Fabricated Structures*, ASM.

**Table 3**  $T_0$  Results for C(T) and SE(B) Placed in “Bins”

Bin ID	C(T)			SE(B)		
	N	r	$T_0$ °C	N	r	$T_0$ °C
A	-	-	-	-	-	-
B	4	1	-	17	9	-118.8
C	31	29	-79.4	24	23	-89.5
D	12	12	-69.1	21	18	-90.3
E	-	-	-	-	-	-
F	16	14	-69.3	34	33	-85.2
G	38	35	-77.7	25	21	-96.3
H	10	10	-74.2	-	-	-
I	-	-	-	-	-	-

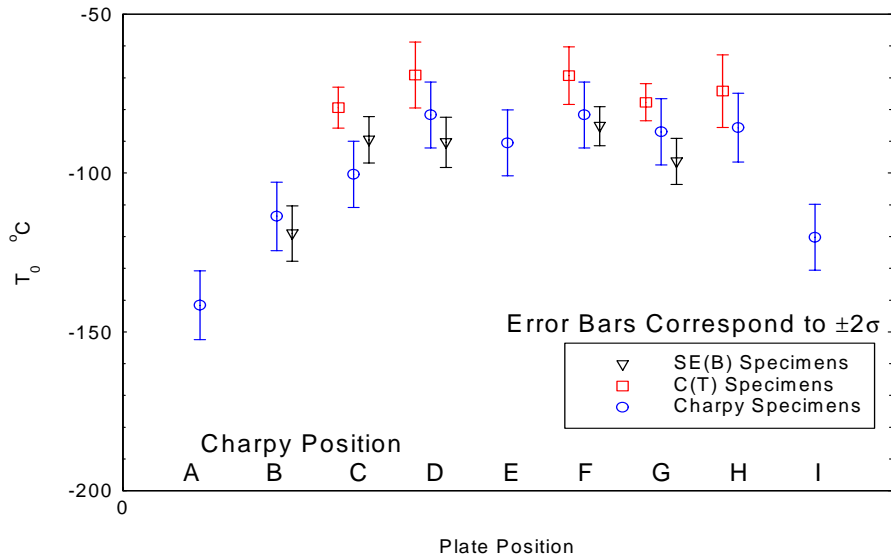


**Figure 5**  $T_0$  versus crack position for the three test geometries.